Journal of Japan Association for Earthquake Engineering, Vol.15, No.3, 2015

DAMAGED STORY DETECTION AND MODAL PROPERTIES OF A RC BUILDING SUBJECTED TO 2011 TOHOKU EARTHQUAKE

Kahori IIYAMA[1], Satoshi KURITA[2] , Masato MOTOSAKA[3] ,
Kazuki CHIBA[4], Yuta SAKURADA[5] and Kazuya MITSUJI[6]

[1] Member of JAEE, Researcher, Information Science and Engineering, Tokyo Institute of Technology, Tokyo, Japan, iiyama.k.aa@m.titech.ac.jp
[2] Member of JAEE, Professor, Department of Architecture, Tokyo University of Science, Tokyo, Japan, kurita@rs.kagu.tus.ac.jp
[3] Member of JAEE, Professor, International Research Institute of Disaster Science, Tohoku University, Miyagi, Japan, motosaka@irides.tohoku.ac.jp
[4] Member of JAEE, Researcher, Tokyu Construction Co., Ltd., Institute of Technology, Kanagawa, Japan, chiba.kazuki@tokyu-cnst.co.jp
[5] Member of JAEE, Dai-ichi Building Co., Ltd., Tokyo, Japan, sakura.d.yuta@gmail.com
[6] Member of JAEE, Associate Professor, Department of Education, Art and Science, Yamagata University, Miyagi, Japan, mitu@e.yamagata-u.ac.jp

ABSTRACT: The modal properties of a three-story reinforced concrete building that was affected by the 2011 Tohoku Earthquake were revealed through acceleration records of the main shock and ambient vibration. Damaged stories were detected from identified natural modes from the records. In addition, we estimated the modal parameters using two types of frequency domain decomposition techniques: one for a general viscous damping system and the other for a proportional damping system. The influence of the viscous damping condition on the identified natural modes was discussed.

Key Words: Microtremor measurement, Damage estimation, System identification, Frequency domain decomposition

1. INTRODUCTION

After the 1995 Hyogoken-Nanbu (Kobe) Earthquake, techniques for structural health monitoring were developed. Some techniques of damage detection are based on the methods which use vibrational records measured on structures, and their effectiveness has been verified by numerical and laboratory tests. However, although the analysis of the vibrational characteristics of actual building experienced huge earthquakes are necessary to find effective damage indicators, such studies are limited. From the authors' point of view, studies based on the measurements of a damaged building are very important.

In this study, the modal properties of a three-story reinforced concrete (RC) building affected by the 2011 Tohoku Earthquake were identified through a high-density array measurement of the ambient vibration, and the damaged stories were estimated using a conventional technique. The specific advantages of using the building were that forced vibrational tests and measurements have been conducted several times[1-4], and many earthquake response records have been accumulated using the observation system installed in the building. This paper is outlined as follows. First, the records of the main shock were analyzed, and the seismic intensity, maximum deformation, and change in natural frequency before and after damage were examined. Second, the modal properties were identified using frequency domain decomposition (FDD) techniques from the ambient vibration data obtained after the main shock. One of the FDD techniques is a conventional technique[5] that is applied to a nonproportional damping system, and the other is an extended technique[6] that is applied to a proportional damping system. Using the two FDD techniques, the viscous damping system of the damaged building under small-amplitude vibrations was discussed. From the identified mode shapes, the location of the damaged story was estimated. Finally, by using past studies and accumulated response records, the relation between the change in frequency and damage was examined.

2. DAMAGE FROM 2011 TOHOKU EARTHQUAKE

2.1 Building outline

The objective building was constructed for experimental purposes at the campus of Tohoku University in May 1986 (Photo 2.1). The elevation and the plan of the first floor are shown in Fig. 2.1. The non-

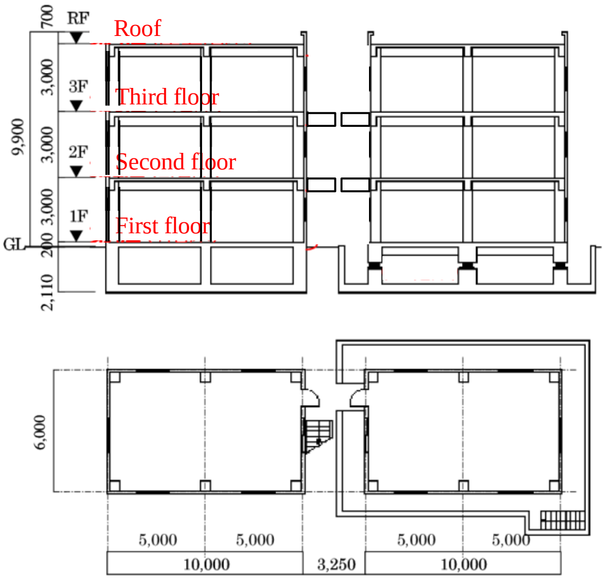

Figure 2.1. (a) Elevation, (b) plan (units in mm)
(Left: NIB; right: IB)

Photo 2.1. Objective building
(Left: NIB; right: IB)

Table 1. Cross section sizes of girders and columns (unit: mm×mm)

	Girder	Column
Roof	300×550	---
Third floor	300×600	500×500
Second floor	300×600	500×500
First floor	---	500×500

isolated building (NIB) and isolated building (IB) are adjacent, as shown in Photo 2.1 and Fig. 2.1; mainly the former was used in this study. The plan dimensions are 6.0 m × 10.0 m, and the height of each story is 3.0 m.

The dimensions consist of a regular frame structure in the transverse (N–S) and longitudinal (E–W) directions. The external walls of the building are autoclaved lightweight aerated concrete (ALC) panels. The strength of the concrete is 210 kg/cm^2, and the reinforcing steels are SD30 and SD35. The cross-sectional sizes of the girders and columns are listed in Table 1, and the thickness of the floor slab is 135 mm. The type of basement is a spread foundation, and the ground soil type is classified as II. There are common steel stairs between the two buildings, and the landings have a clearance of 45 mm.

2.2 Building damage

The damage inspection of the building was performed in September 2011 (6 months after the Tohoku Earthquake). The findings are summarized as follows:

1) Outer walls

Several small failures, as shown in Photo 2.2, were found near the corners of the ALC panels in both the transversal and longitudinal sides. According to the design guideline,[8] the extent of the damage corresponded to a degree of C, which means that the panel does not need to be replaced, but the seals need to be repaired.

2) Columns

Plural flexural cracks with widths of 0.1–0.3 mm were observed on the columns. Parts of the cracks traced by white chalk are shown in Photo 2.3. Similar cracks were found in all stories, and some of them seemed to be deep enough to reach the inner steel rods. According to the technical guideline,[9] the extent of the damage corresponded to Level II.

3) Girders

Similar to the columns, plural flexural cracks with widths of 0.1–0.3 mm were observed on the girders, and the extent of the damage corresponded to Level I or II. Parts of the cracks traced by white chalk are shown in Photo 2.4. Similar cracks were found in all stories, and some of them reached the girder height.

The failures in the outer walls were likely caused by the Tohoku Earthquake because they had not been observed before the earthquake. However, the origin of the cracks on the girders and columns was uncertain because a crack inspection had not been conducted before the earthquake.

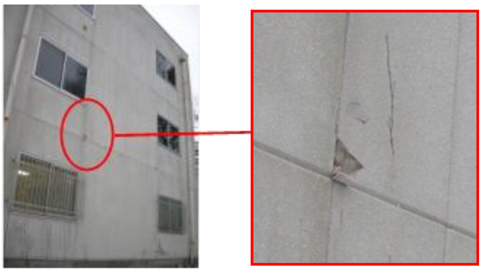

Photo 2.2. Damage on external wall.

Photo 2.3. Cracks on column.

Photo 2.4. Cracks on girder.

3. ANALYSIS OF EARTHQUAKE RECORDS

3.1 Earthquake observation and records

In the NIB and IB, accelerations (37 components), displacements (two components), and temperature were observed at 20 observation points.[3)] Only the points used in this study are shown in Fig. 3.1. In the NIB, accelerograms were installed on the first floor and on the roof. The time histories of the response acceleration observed during the main shock of the Tohoku Earthquake are shown in Fig. 3.2, and the maximum acceleration and seismic intensity are shown in Table 3.1. The maximum accelerations in the transversal (*TR*) and longitudinal (*LG*) directions were approximately 300 cm/s^2 at the first floor, and a seismic intensity of 5.5 was registered. At the roof, maximum accelerations of 702 cm/s^2 and 824 cm/s^2 in the *TR* and *LG* directions, respectively, were observed.

To estimate the strength of the main shock, the acceleration response spectra, which were calculated from the records of the first floor, are shown in Fig. 3.3 for both directions. In addition, the damage limit acceleration spectrum and safety limit acceleration spectrum for a ground type of II, which was calculated from the abbreviated formula for the amplification factor (Gs) of the surface gr-

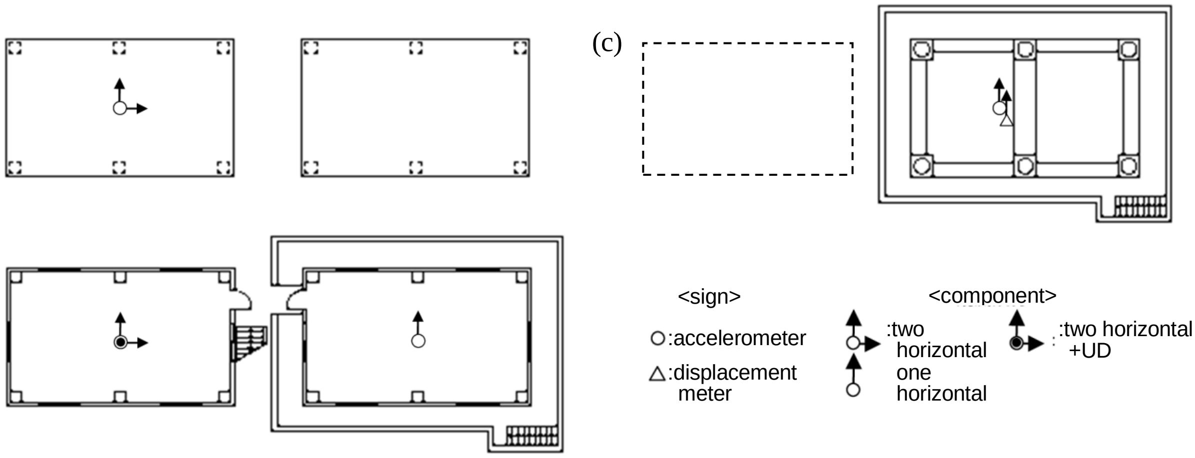

Figure 3.1. Location of observation points used in this study (left: NIB; right: IB): (a) roof, (b) first floor, and (c) basement floor

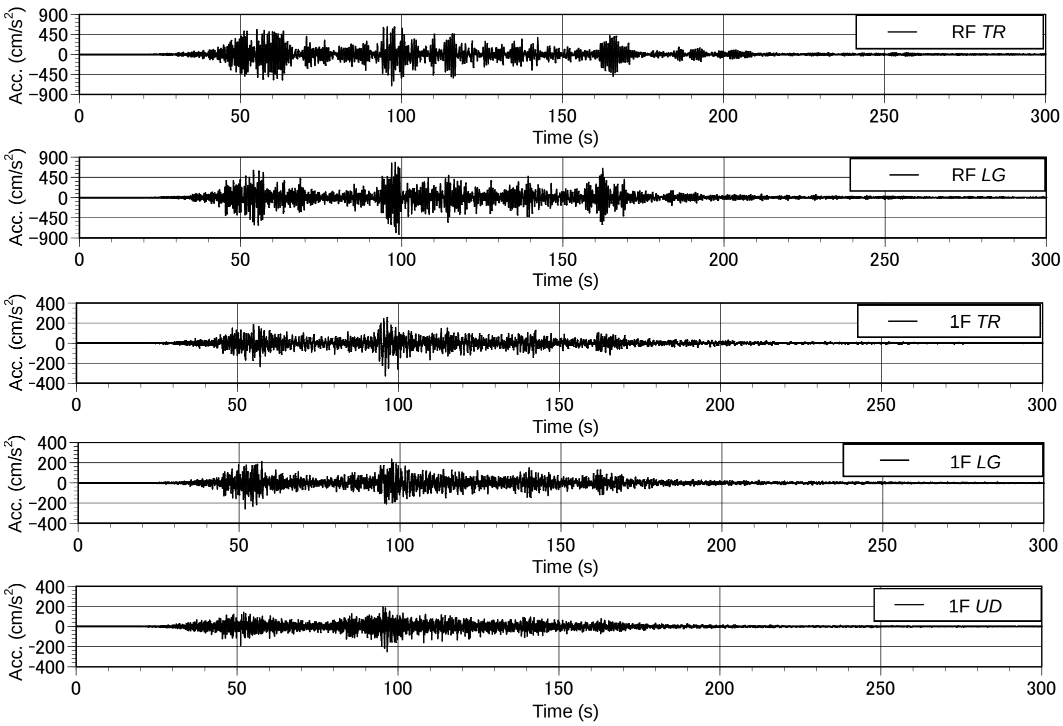

Figure 3.2. Acceleration time history for main shock of the 2011 Tohoku Earthquake observed in the NIB

Table 3.1. Maximum acceleration and seismic intensity for the 2011 Tohoku Earthquake observed in the NIB

Location	Direction	Maximum acceleration (cm/s^2)	Seismic intensity
RF	*TR*	702	
	LG	824	
1F	*TR*	327	5.5
	LG	258	
	Up-down(*UD*)	220	

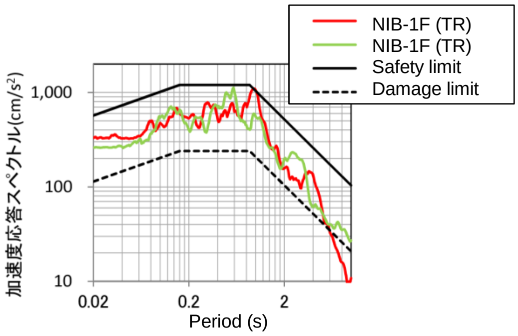

Figure 3.3. Acceleration response spectra at the first floor of the NIB

ound, are also shown in Fig. 3.3. In the range from 0.2 to 0.3 Hz, which nearly corresponds to the natural frequency of the building, both the acceleration response spectra are large enough to reach approximately three times the damage limit acceleration spectrum.

3.2 Maximum deformation of building

The maximum deformation of the NIB was estimated from the displacement time records, which were calculated by differentiating the acceleration time records shown in Fig. 3.2. Katsukura's technique[10), 11)] was applied to the differentiation; then, the noises included in the long period range were purged by a low-cut filter. To take the Fourier spectrum shown in Fig. 3.4 at the first floor of the NIB for the *TR* direction as an example, the cutoff frequency f_c for the low-cut filter was determined to be 0.2 Hz because the Fourier spectrum decreased to approximately 0.2 Hz, and a frequency range lower than 0.2 Hz was regarded as noise. A frequency range higher than 0.2 Hz was used to integrate the acceleration to obtain the displacement. To check the accuracy of the numerically integrated displacement, the relative displacement of the isolated layer for the IB was compared to the displacement record directly observed by the displacement meter on the building, as shown in Fig. 3.5. The blue and red lines in the figure are the numerically integrated displacement waveform and the observed waveform, respectively. The integrated displacement waveform corresponded approximately to the observed record. As the difference between the two waveforms was approximately 3.6% (Table 3.2), the numerical integration was sufficiently accurate.

The relative displacement waveforms of the roof to the first floor, which were calculated by the integral of each acceleration observed on the NIB, are shown in Fig. 3.6. As shown in Table 3.3, the maximum value for the *TR* direction was 5.5 cm, which was larger than that for the *LG* direction of 4.74 cm. The maximum angle of deformation was obtained by dividing the maximum displacement by

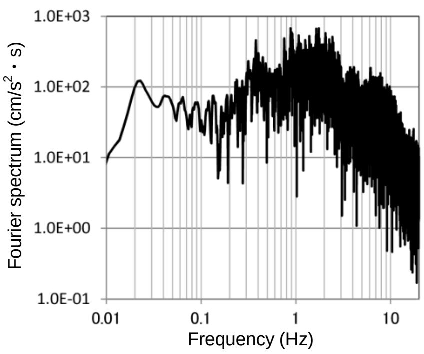

Figure 3.4. Acceleration fourier spectrum in *TR* direction at the first floor of NIB

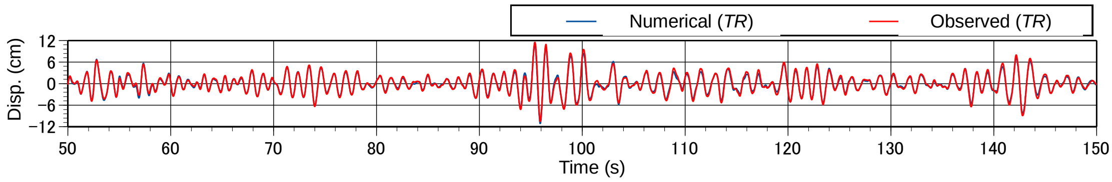

Figure 3.5. Validation of numerical integration using the observed records on IB (relative displacement of isolated layer)

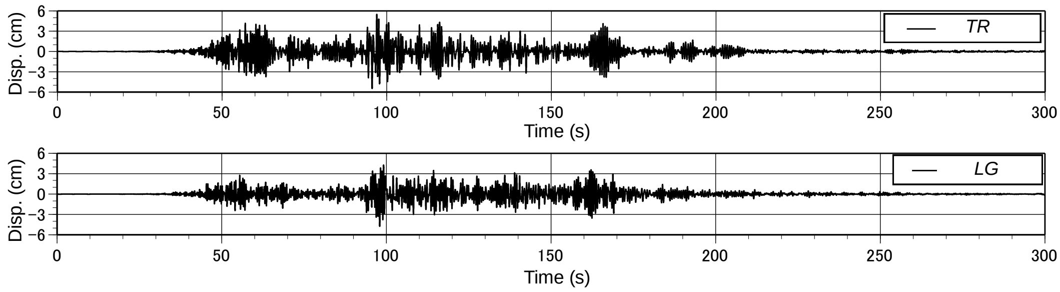

Figure 3.6 Calculated relative displacements at roof to the first floor (NIB)

Table 3.2. Comparison of maximum displacement at base isolated layer (*TR*)

Method	Maximum displacement(cm)
Numerical integral	11.1 (1.000)
Observation records	11.5 (1.036)

Table 3.3. Maximum relative displacement and maximum distortion angle calculated from acceleration records

Direction	Maximum relative displacement(cm)	Maximum distortion angle
TR	5.50	1/164
LG	4.74	1/190

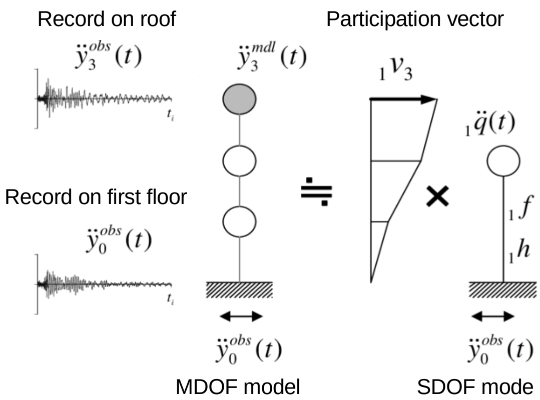

Figure 3.7. Schematic diagram of system identification using modal model

Table 3.4. Identified modal property of first order mode and maximum acceleration at roof

		Initial interval	End edge interval	End /initial
TR	Eigenfrequency(Hz)	2.90	1.80	0.62
	Damping factor	1.66%	5.86%	3.53
	Participation factor	1.23	1.16	0.94
	Maximum acceleration at roof (cm/s^2)	10.9	13.8	1.27
LG	Eigenfrequency(Hz)	3.49	2.00	0.57
	Damping factor	4.61%	9.97%	2.16
	Participation factor	1.23	1.30	1.06
	Maximum acceleration at roof (cm/s^2)	7.81	17.2	2.20

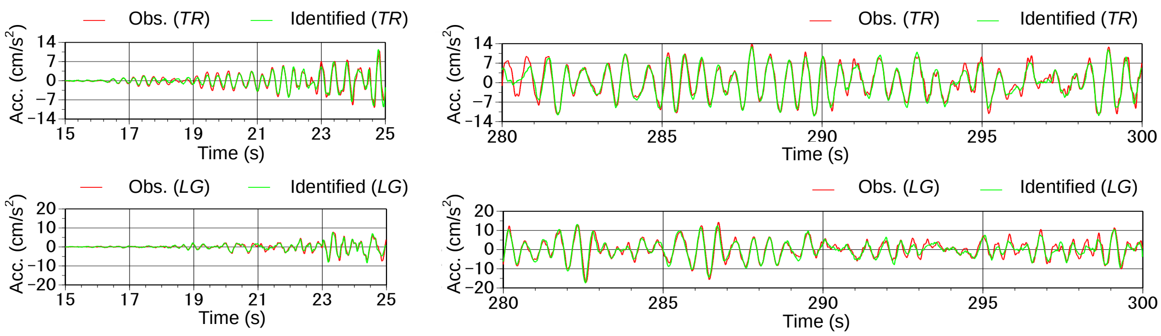

Figure 3.8. Comparison between observed acceleration record and acceleration wave calculated by system identification (on the roof of the NIB)

the height of 9.0 m and is shown in Table 3.3. The maximum angles for the *TR* and *LG* directions were 1/164 and 1/190, respectively. Thus, the NIB was globally deformed enough to exceed the limited value of 1/200, which means that the nonstructural elements and equipment were possibly damaged.

3.3 Change in modal properties

A change in the modal properties before and after the main shock was examined. The modal properties were identified from the initial and end edge intervals of the acceleration record. A summary of the system identification is shown in Fig. 3.7. A model with a single degree of freedom (SDOF) for a proportional damping system was employed in the identification by entering the horizontal acceleration record $\ddot{y}_0^{obs}(t_i)$ of the first floor in the modal model and computing the horizontal acceleration response $\ddot{y}_3^{mdl}(t_i)$ at the roof. Then, the modal properties (the first-order eigenfrequency ${}_1f$, damping factor ${}_1h$, and participation vector ${}_1\nu_3$) were obtained using a modified Gauss–Newton method by minimizing the following square error J.

$$J = \sum_{t_i=t_b}^{t_f} \left(\ddot{y}_3^{mdl}(t_i) - \ddot{y}_3^{obs}(t_i) \right)^2 \qquad (t_b,\ t_f\text{: Start time and end time of the target interval}) \qquad (3.1)$$

A Newmark β method was applied to the response analysis. The modal properties were identified for two intervals of the acceleration record shown in Fig. 3.2: 15–25 s (initial interval) and 280–300 s (end edge interval).

The identified modal properties for the first-order mode are shown with the maximum acceleration of each interval in Table 3.4. Because the maximum acceleration is less than 20 cm/s^2, the building vibration can be determined using a linear system. Comparisons between the observed acceleration record and the acceleration wave calculated by the system identification are shown in Fig. 3.8. According to the figure, the identification results agree well with the observation records—that is, the identification accuracy is high. The identified frequencies are 2.90 Hz and 3.49 Hz for the *TR* and *LG* directions, respectively, for the initial interval of the acceleration records. However, the frequencies for the end edge interval are 62% and 57% of that for the initial interval, respectively. The results indicate that the building was severely damaged by the main shock and that the stiffness greatly decreased. In addition, because the amount of reduction for the *TR* direction was slightly larger than that for the *LG* direction, the damage for the *TR* direction was probably more severe than that for the *LG* direction.

The damping factor for the end edge interval increased several times from the initial interval; however, the participation function did not show such a difference.

4. MODAL IDENTIFICATION AND DAMAGE ESTIMATION BASED ON AMBIENT VIBRATION

4.1 High-density array measurement of ambient vibration

A simultaneous high-density array measurement of the ambient vibration was performed on September 15, 2011. We used two types of portable accelerometers: GPL-6A3P (Mitutoyo Co.) and

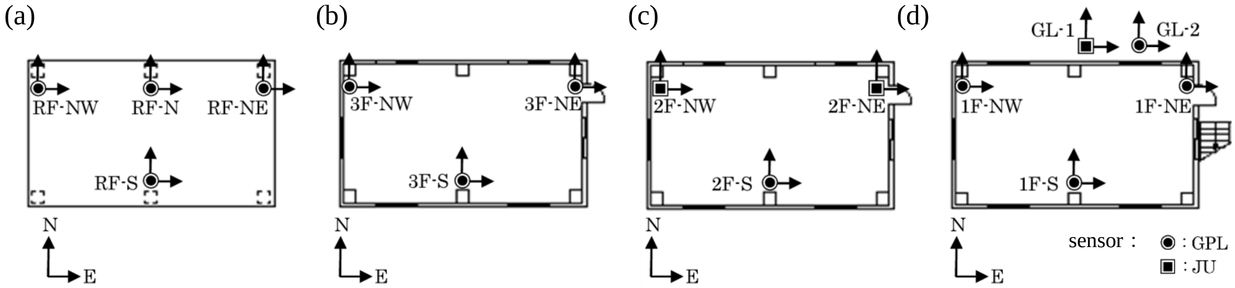

Figure 4.1. Location of portable accelerometers in the simultaneous array measurement : (a) roof, (b) third floor, (c) second floor and (d) first floor

JU (Hakusan Co.). To obtain multi-dimensional mode shapes of the damaged building, three accelerometers were installed on every floor, as shown in Fig. 4.1. All the accelerometers measured two horizontal components (x and y directions) and a vertical component (z direction). The inner clocks of the accelerometers were synchronized using a GPS system just before the measurement. The ambient vibrations were recorded continuously for 30 min at a sampling frequency of 200 Hz.

According to the anemometer on the roof of a 56m-high building that is located several hundred meters away from the building, the 10 minutes average wind velocity was 0.40 - 0.50m/s and the maximum wind velocity was 1.68 m/s during the measurement.

4.2 Identification method

The modal parameters of the building were identified using FDD techniques. To examine the damping system of the building at an ambient vibration level, two different FDD techniques were introduced. The first was a technique for a nonproportional damping system[5)] (hereafter called the *conventional method*), and the second is a technique for a proportional damping system[7)] (hereafter called the *proposed method*).

Both techniques use the power spectrum matrix $[G(j\omega)]$. The symbol $y_i(t)$ denotes the response time series data at the measurement point i (i = 1, …, N). Using the response column vector $Y_i(j\omega)$, which is the Fourier transform of $y_i(t)$, $[G(j\omega)]$ is defined by the following:

$$[G(j\omega)] = E[\{\overline{Y}(j\omega)\}\{Y(j\omega)\}^T] \tag{4.1}$$

where ω is the circular frequency. The symbols E, j, $\bar{\ }$, and superscript T denote the ensemble average, the imaginary unit, a complex conjugate, and a transposition, respectively. Let N be the total number of measurement points; $\{Y(j\omega)\}$ is represented by

$$\{Y(j\omega)\} = \{Y_1(j\omega),...,Y_N(j\omega)\}^T \tag{4.2}$$

In Brincker et al.'s technique (conventional method), the complex conjugate matrix of $[G(j\omega)]$ is decomposed by taking the singular value decomposition as follows:

$$[\overline{G}(j\omega)] = [U(j\omega)][S(j\omega)][U(j\omega)]^H = \sum_{i=1}^{N} s_i(j\omega)\{U_i(j\omega)\}\{U_i(j\omega)\}^H \tag{4.3}$$

where the superscript H represents the complex conjugate and transposition, and $s_i(j\omega)$ and $\{U_i(j\omega)\}$ are the ith singular value and corresponding singular vector, respectively. Here, let the maximum singular value be $s_1(j\omega)$ (the first singular value) and the corresponding vector be $U_1(j\omega)$ (the first singular vector). Supposing that the inputs are white noise, $[G(j\omega)]$ in the vicinity of the rth natural frequency ω_r can be approximated as the following equation:

$$[\overline{G}(j\omega)] \approx a_r(j\omega)\{\Phi_r\}\{\Phi_r\}^H,\ a_r(j\omega) = \mathrm{Re}\left(\frac{2d_r}{j\omega - \lambda_r}\right) \tag{4.4}$$

where λ_r is the pole for ω_r and is represented by the modal damping ratio σ_r and damped natural circular frequency ω_{dr} as follows:

$$\lambda_r = -\sigma_r + j\omega_{dr} \tag{4.5}$$

where d_k is a scalar relevant to white noise excitation, and $\{\Phi_r\}$ denotes the complex rth-order mode shape vector. Comparing Eqs. (4.3) and (4.4), the first singular value and vector corresponds to a_r and $\{\Phi_r\}$, respectively. From the correspondence relation, the rth-order mode can be identified from the corresponding singular vector to the rth peak frequency of a_r. Further, the rth-order natural frequency and modal damping factor are identified from the damped oscillatory wave, which is obtained by the inverse Fourier transform of a_r around the rth peak frequency.

Iiyama and Kurita[7)] reconstructed the theoretical background of the conventional method[5)] to clarify the influence of existing closely spaced modes on the modal identification results. Furthermore, they proposed a FDD technique for proportional damping systems that uses only the real part of

$[G(j\omega)]$. Considering that $[G(j\omega)]$ is a Hermitian matrix,[12] they applied spectral decomposition as a matrix decomposition method.

$$[G^R(j\omega)] = [P(j\omega)][Q(j\omega)][P(j\omega)]^T = \sum_{i=1}^{N} q_i(j\omega)\{p_i(j\omega)\}\{p_i(j\omega)\}^T \tag{4.6}$$

where the superscript R denotes the real part of a complex number or matrix, and $q_i(j\omega)$ and $\{p_i(j\omega)\}$ are the ith eigenvalue and eigenvector at ω, respectively. Here, let the maximum eigenvalue be $q_1(j\omega)$ (the first eigenvalue) and the corresponding vector be $p_1(j\omega)$ (the first eigenvector). For a proportional damping system subjected to white noise, $[G^R(j\omega)]$ is approximated as follows around the rth natural frequency ω_r:

$$[G^R(j\omega)] \approx 2a_{rr}^p(j\omega)\left(\{\phi_r\} + \{\Delta_r^R(j\omega)\}\right)\left(\{\phi_r\} + \{\Delta_r^R(j\omega)\}\right)^T \tag{4.7}$$

where

$$a_{rr}^p = \frac{c_{rr}}{2\left(\sigma_r^2 + (\omega - \omega_{dr})^2\right)}, \tag{4.8}$$

c_{rr} represents a constant value relevant to the input white noise, $\{\phi_r\}$ is the rth-order eigenmode (real number), and $\{\Delta_r^p(j\omega)\}$ represents an error vector[7] with respect to the closely spaced modes $\{\phi_s\}$ $(s \neq r)$, which takes the minimum value at $\omega = \omega_{dr}$ and a larger value with a larger difference between ω_{dr} and ω_{ds} $(s \neq r)$.

4.3 Modal identification

The elements of the $[G(j\omega)]$ matrix, the frequency response function (FRF), and the coherence function (COF) were calculated from the ensemble average of 20 sample waves, which were continuously cut from the records. The number of data points in a sample wave was 16,384.

4.3.1 Property of accelerometer

Because two types of accelerometers (GPL and JU) were used in this study, the difference between the accelerometers in terms of the frequency response characteristics should be verified. As examples, the COF and FRF were calculated by setting the record at Location GL-2 (GPL) as an input and the record at GL-1 (JU) as an output. The results are shown in Figs. 4.2(a) and (b). Both the COF and amplitudes of FRF were approximately 1.0 for the range of 3–10 Hz.

However, the phase of the FRF had a linear slope [Fig. 4.2(c)], which indicated that there is a small time lag between the inner clocks of each accelerometer. Although the inner clocks of all accelerometers were synchronized using a GPS system just before being set up at each location, the time delays of the clocks probably progressed because it took approximately 4 h to start the measurements. The optimal relative time lag τ_0 can be calculated by fitting the phases to $\theta(f) = 2\pi\tau_0 f$ by the least-squares method in the straight-line frequency range. The time lag calculated for the range of

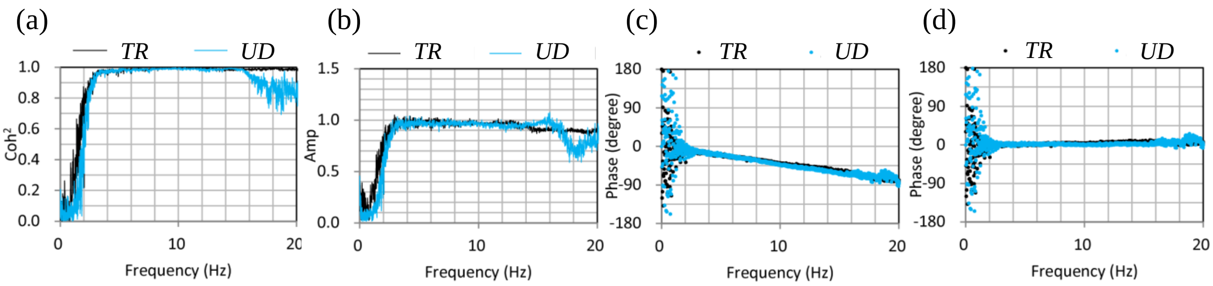

Figure 4.2. Comparison of frequency characteristics between two types of accelerometers: (a) COF, (b) amplitude of FRF, (c) phase of FRF (before time correction), and (d) phase of FRF (after time correction)

5–15 Hz of Fig. 4.2(c) was −0.0116 s. Fig. 4.2(d) shows the phases after the time correction. The phases were approximately equal to zero at a frequency range lower than 15 Hz.

4.3.2 Time correction of accelerometer

Because Fig. 4.2(c) indicates that the time delays of the inner clocks of the accelerometers gradually progressed during the measurements, the time lags between all accelerometers were corrected using the same process discussed in Section 4.3.1. The relative time lags between the records were calculated using the records in the up–down (*UD*) directions because they can be calculated using the frequency range in which the phase values are approximately 0 degrees. Generally, the range from 0 Hz to the first natural frequency is approximately 0 degrees, and the range for the *UD* direction is wider than that for the horizontal direction in this measurement. Figs. 4.3(a) and (b) show the amplitude and phase of the FRF on the roof for the first floor at Location S for the horizontal and *UD* directions. According to Fig. 4.3(a), the first natural frequency for the *UD* direction is approximately 16 Hz and is much larger than that of 2.2 Hz for the horizontal direction. Fig. 4.3(b) shows that the phases for the *UD* direction linearly increase to 14 Hz, except for approximately 8 Hz, which is considered to be the second-order mode in the *TR* direction. Then, the time lags were calculated using the range from 3.0 to 7.0 Hz of the record for the *UD* direction. The minimum and maximum time lags were −0.00930 s and 0.0298 s, respectively. The phases of the FRF after the time correction are shown in Fig. 4.3(d).

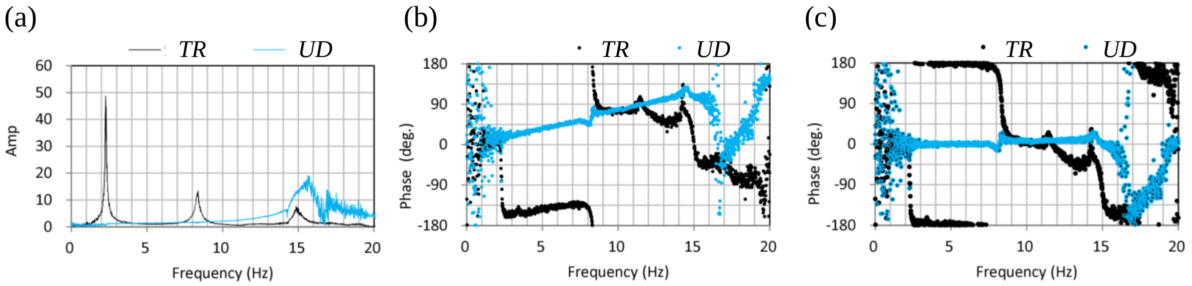

Figure 4.3. Frequency response function on the roof for the first floor (Location S): (a) amplitude of FRF, (b) phase of FRF before time correction, and (c) phase of FRF after time correction

4.3.3 Identification of eigenmode

The modal frequencies and mode shapes of the structure were identified using the horizontal acceleration data at Locations S, NE, and NW shown in Fig. 4.1. The total number of measurement points was 12. Each element of the power spectral matrix ($[G(j\omega)]$ or $[G^R(j\omega)]$) was corrected using the calculated time lags in Section 4.3.2. A comparison between the first singular value for the conventional method (singular value spectrum) and the first eigenvalue for the proposed method (eigenvalue spectrum) is shown in Fig. 4.4, where σ and the subscript indicate the singular value or the

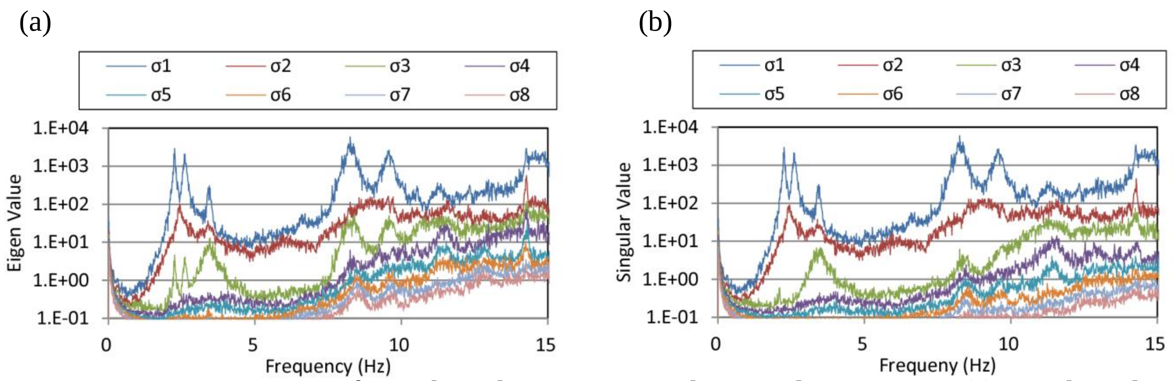

Figure 4.4. Comparison of singular value spectrum and eigenvalue spectrum: (a) singular value spectrum (conventional method), (b) eigenvalue spectrum (proposed method)

eigenvalue and its order. Only the first to eighth orders are shown in the figure. The first and second orders of the eigenvalues and singular values are almost the same, and their first orders have peak frequencies of 2.26, 2.59, 3.44, 8.25, and 9.58 Hz.

Fig. 4.5 shows the singular vectors (complex modes) for the conventional method and the eigenvectors (real modes) for the proposed method at the aforementioned five frequencies at the horizontal Locations NE and NW. The upper panels show the mode vectors for the *TR* direction and the lower panels for the *LG* direction. The vertical axes show the floor number. The mode vector is normalized with respect to the highest value among all nodes. All the modes in Fig. 4.5 and the real parts of the complex modes seem to agree with the real mode vectors. In addition, although the imaginary parts of the complex modes take small (non-zero) values in the *LG* direction at 3.44 Hz and in the *TR* direction at 8.25 Hz, most of them are nearly equal to zero.

According to the eigenvectors, we can identify the vector at 2.26 Hz as the first translational mode for the *TR* direction, at 2.59 Hz as the first translational mode for the *LG* direction, at 3.34 Hz as the first torsional mode because the eigenvector at Location NE moves to the opposite direction (Fig. 4.6) for the eigenvector at Location NW, at 8.25 Hz as the second translational mode for the *TR* direction,

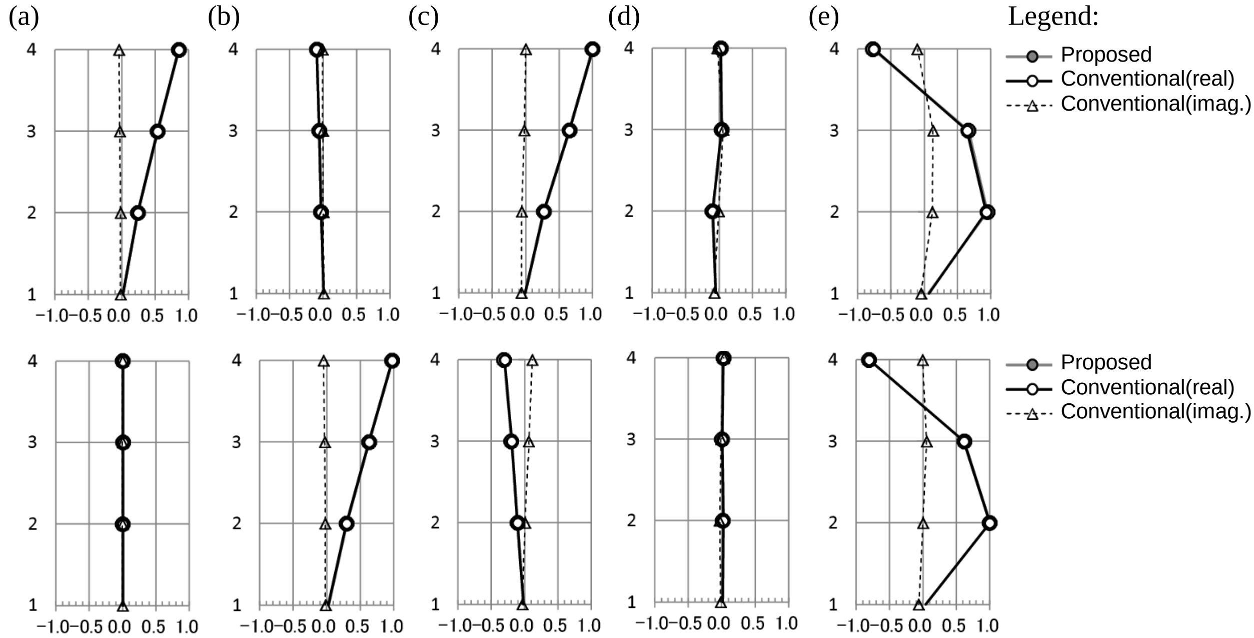

Figure 4.5. Comparison of singular vector and eigenvector at Location NW: (a) 2.26Hz, (b) 2.59Hz, (c) 3.44Hz, (d) 8.25Hz, and (e) 9.58Hz (upper figure for *TR* direction and lower figure for *LG* direction)

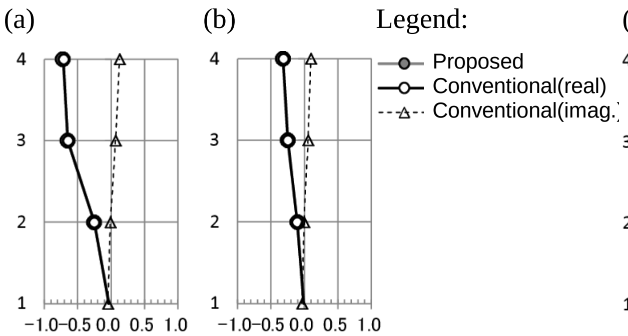

Figure 4.6. Eigenmode at location NE (3.44 Hz): (a) *TR* direction and (b) *LG* direction.

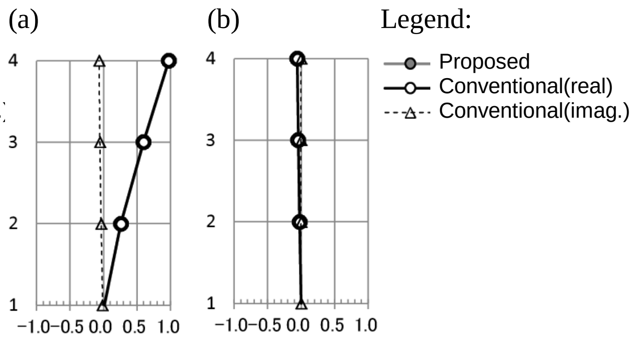

Figure 4.7. Eigenmode at location NE (3.44 Hz): (a) *TR* direction and (b) *LG* direction.

and at 9.58 Hz as the second translational mode for the *LG* direction.

Although the FRF showed different properties between the accelerometers GPL and JU in a frequency range lower than 3 Hz, there is no difference between the eigenvectors on the second layer at Location S (Fig. 4.7, GPL) and that at Location NW [Fig. 4.5(a), JU] for 2.26 Hz. Therefore, it is believed that the difference of the properties between GPL and JU probably does not affect the identification results.

4.3.4 Identification of eigenfrequency and modal damping factor

The modal damping factors for each mode were identified using the two FDD techniques. The results are listed in Table 4.1. There are no differences between the two methods because the first singular values are in good agreement with the first eigenvalues, as shown in Fig. 4.4. All of the damping factors were in the range of 1.3–1.9%, which is as low as those of the undamaged RC buildings. Regarding the first-order translational mode, the value for the *LG* direction was slightly larger than that for the *TR* direction. However, regarding the second-order translational mode, the value for the *LG* direction was approximately the same as that for the *TR* direction.

Table 4.1. Comparison of natural frequency and modal damping factor

Component and order of eigenmode		Natural frequency (Hz)		Modal damping factor (%)	
		Proposed	Conventional	Proposed	Conventional
TR	First order (translational)	2.25	2.25	1.32	1.32
	Second order (translational)	8.26	8.26	1.46	1.46
LG	First order (translational)	2.60	2.60	1.87	1.87
	Second order (translational)	9.57	9.57	1.47	1.47
First order (torsional)		3.42	3.42	1.59	1.59

4.4 Estimation of damaged story based on change in eigenmode

The application to damage story detection—the mode shape curvature—was calculated from the measured mode shapes. In this method, the damaged story is determined from the difference of the mode shape curvatures before and after damage.

The mode shape curvature was defined by using the one-dimensional in-line multiple degree of freedom model. Let the *i*th order eigenmode on the *j*th story be $\phi_{i,j}$; the curvature C_{ij} is given by using a central difference approximation:

$$C_{ij} = (\phi_{i,j-1} - 2\phi_{i,j} + \phi_{i,j+1}) / h^2 \tag{7}$$

where h is the distance between the floors. Here, the changes in the curvature after the occurrence of damage[13)] are defined as

$$CURV_{ij} = \left| C_{ij,t} - C_{ij,0} \right| \tag{8}$$

where $C_{ij,0}$ and $C_{ij,t}$ are the mode shape curvatures before and after damage, respectively.

Because the authors did not measure the vibrational records before the Tohoku Earthquake, we made the three-dimensional frame model based on the structural calculation sheets and calculated the mode shape by using the frame model, which is regarded as the mode shape before damage. Therefore, *CURV* represents the accumulated damage from the completed construction.

The natural frequencies calculated using SEIN La CREA—software created by NTT Data Co.—are shown in Table 4.2. To check the accuracy of the three-dimensional frame model based on the structural calculation sheets, the natural frequencies for the first-order translational mode calculated by the forced vibration test conducted just after the completion construction are shown together. Although there is a small difference between the frequencies for the second-order mode, the frequencies for the first mode are in good agreement. Fig. 4.8 shows the comparison of the translational mode shapes between the frame model (as the undamaged mode) and the identified mode (as the damaged mode), which represent the mode value at the center of mass and were normalized such that the maximum value was 1.0. The identified modes of each story were calculated from the modes at the three locations on each floor by the least-squares method under the assumption that the floor was sufficiently rigid. According to the figure, regardless of the directions, the differences between the modes seem to be negligibly small. However, the *CURV* values calculated for h = 3 m are shown in Fig. 4.9. The difference of *CURV* between the second and third floors is very small, except for the first mode in the *TR* direction. With respect to the *LG* direction, $CURV_{13}$ is slightly larger than $CURV_{12}$. However, $CURV_{23}$ is slightly smaller than $CURV_{22}$. It can be seen that the damage is not concentrated in specific floors—i.e., all the floors were similarly damaged. During the crack inspection, plural flexural cracks were discovered on all floors, and the number and length of the cracks were nearly equal in each floor. Thus, the changes in curvature seem to explain the damaged conditions that were found in the damage investigation.

Table 4.2. Result of eigenvalue analysis

Eigenmode	Eigenfrequency (Hz)	
	First-order mode	Second-order mode
Translational mode for *TR* direction	3.59 (3.63)	11.8
Translational mode for *LG* direction	3.90 (4.39)	12.4
Torsional mode	4.02	12.9

The values in parentheses are the natural frequency based on the forced vibration test conducted just after the completion of construction.

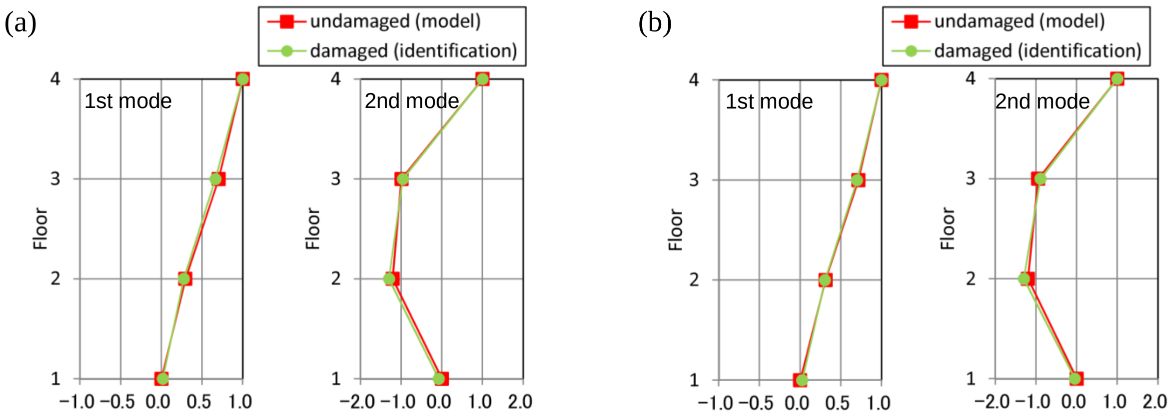

Figure 4.8. Translational mode shapes for undamaged (frame model) and damaged (identification): (a) *TR* direction; (b) *LG* direction

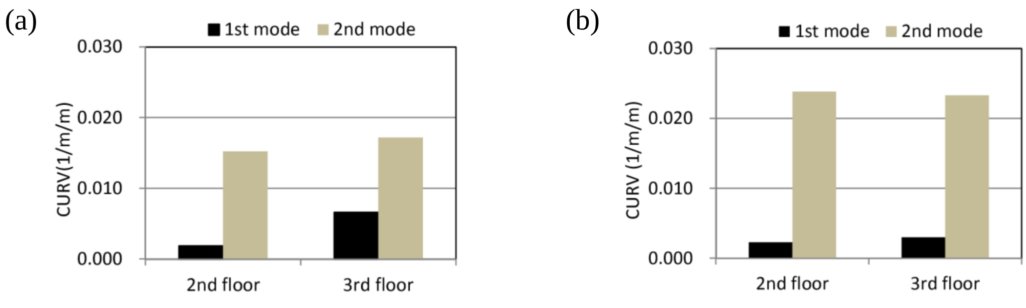

Figure 4.9. Changes in curvature between undamaged mode and damaged mode: (a) *TR* direction; (b) *LG* direction

5. DISCUSSION

According to the analysis from the records of the main shock, the acceleration response spectra of the first floor reached approximately three times the damage limit acceleration spectrum in a range that nearly corresponds to the natural frequency of the building. In addition, the maximum angles exceeded the limited value of 1/200. Based on the results, it is very probable that the main reinforcement of the column and beams yielded from the Tohoku Earthquake. The identified modal properties and the results of damage detection are discussed in this section.

5.1 Relation between change in natural frequency and damage

The change in frequencies of the first-order mode (hereafter called f_{1amb}), which were obtained from the past ambient vibration measurements[14), 15)] and this study, are shown in Table 5.1 and Fig. 5.1. Comparing the values of f_{1amb} on September 15, 2001, and those for just after the completion of construction, the frequency ratio was 56% and 51% in the *TR* and *LG* directions, respectively. However, the values of f_{1amb} in 2006 were 75% of those just after the completion of construction for both directions. Considering these ratios, the building was damaged more severely in the *LG* direction due to the earthquakes occurring from 2006 to 2011. In addition, approximately half of the total reductions of f_{1amb} had already decreased prior to 2006. The causes of these changes were analyzed as follows.

The three main earthquakes occurring prior to the 2011 Tohoku Earthquake are listed in Table 5.2. In the table, the maximum values of the horizontal acceleration and relative displacement observed on the roof of the building are also listed. In addition, the relationship between relative displacement and story shear force of the first floor calculated by the push-over analysis is shown in Fig. 5.2. In the push-over analysis, the frame model (referred to in Section 4.4) was employed, and the horizontal force based on the distribution of external forces, which is regulated in the Japanese Building Standards Act as “Ai distribution”, was added to the model. As shown in Fig. 5.2, the elastic limit of displacement seems to be approximately 0.4 cm. According to Table 5.2, the relative displacements from the Miyagi-ken Nanbu Earthquake in 1998 were largest at 1.73 cm and 1.50 cm in the *LG* and *TR* directions, respectively, which were large enough to exceed three times the elastic limit. Considering

Table 5.1. Change in the first natural frequency estimated from ambient vibration.

	First mode frequency (Hz)	
	TR direction	*LG* direction
Before damage (just after completion of construction)[14)]	4.02 (1.00)	5.11 (1.00)
Measurement in 2006[15)]	3.03 (0.75)	3.81 (0.75)
After damage (September 15, 2011)	2.25 (0.56)	2.60 (0.51)

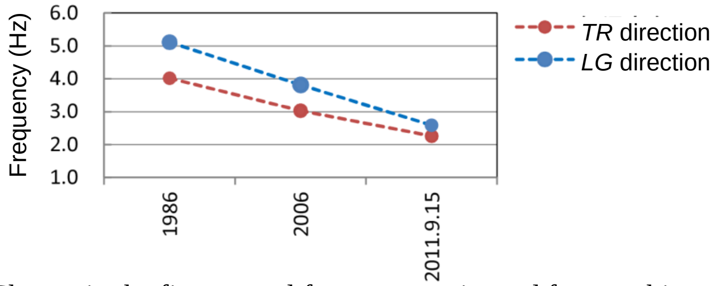

Figure 5.1. Change in the first natural frequency estimated from ambient vibration

Table 5.2. Maximum values of acceleration and relative displacement on roof due to past earthquakes

	Maximum acceleration (cm/s^2)		Maximum relative displacement (cm)	
	TR	*LG*	*TR*	*LG*
Miyagi-ken Nanbu Earthquake in 1998	345	672	1.30	1.73
Miyagi-ken Oki Earthquake in 2003	347	423	1.33	1.50
Iwate-Miyagi Nairiku Earthquake in 2008	230	168	0.98	0.62

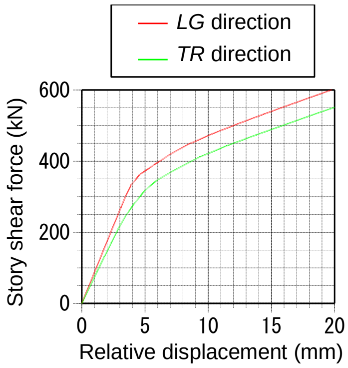

Figure 5.2. Relationship between story shear force and relative displacement (push-over analysis)

that the maximum displacements due to the Miyagi-ken Oki Earthquake in 2003 were approximately the same as or smaller than those due to the Miyagi-ken Nanbu Earthquake, the main cause of the large decrease in f_{1amb} prior to 2006 was probably the Miyagi-ken Nanbu Earthquake in 1998.

However, considering that the maximum displacements due to the Iwate-Miyagi Nairiku Earthquake in 2008 were smaller than those due to the former two earthquakes, it is believed that the decrease in f_{1amb} during 2000–2001 was slight. Therefore, the decrease in f_{1amb}, especially in the *LG* direction, was probably due to the 2011 Tohoku Earthquake. This is reliable because the observation records of the main shock also demonstrated that the change in the first-order natural frequency before and after the earthquake for the *LG* direction was larger than that for the *TR* direction.

5.2 Estimation of damaged story

In Section 4.4, the damaged stories were estimated by using the mode shape curvature calculated from the eigenmodes before and after damage, and the results suggested that all the floors were similarly damaged. However, the past experimental study,[13)] which used the model for which specific stories were damaged, demonstrated that the change in the mode shapes before and after damage was very slight and that the mode changed not locally but globally. Considering these results, it is believed that mode shapes have such a property that they vary slightly and globally if a building has local damage. In this study, the damage level of the selected building was not severe. Therefore, it is unknown whether such a property can also be found in a building that had been very severely damaged.

5.3 Damping property of damaged building at small-amplitude level

By comparing the mode shapes identified from the conventional and proposed methods, the damping system of the existing building under small-amplitude vibrations can be estimated. As shown in Fig. 4.4, the eigenvectors obtained using the proposed method were in agreement with the real parts of the complex singular vectors obtained using the conventional method for all modal orders. However, the imaginary parts of the complex singular vectors obtained using the conventional method were negligibly small in the first modal orders. These results suggest that the damping system of the building can be evaluated as a proportional damping system as far as the lower modes are concerned. The applicability of the proportional damping system to a building more severely damaged is under investigation. In addition, the reason why the imaginary parts took values in some complex modes is also under investigation.

CONCLUSION

This paper discussed a three-story RC building affected by the 2011 Tohoku Earthquake. First, the damage situation was summarized; the records of the main shock were analyzed; and the seismic intensity, maximum deformation, and change in the natural frequency before and after damage were examined. Second, the modal properties were identified using FDD techniques from the ambient vibration data obtained after the main shock. On the basis of the study results, the following conclusions were drawn:

1) According to the damage inspection performed after the 2011 Tohoku Earthquake, the damage on the outer wall was slight. On the column and girder, plural flexural cracks with widths of 0.1–0.3 mm were observed. The extent of the damage shown in a technical guideline corresponded to Level I or II.

2) Based on the analysis of the earthquake response records of the main shock, the acceleration response spectra were large enough to reach approximately three times the damage limit acceleration spectrum in the range of 0.2–0.3 Hz, which is approximately the natural frequency of the building. In addition, from the maximum angles (1/164 and 1/190 for the *TR* and *LG* directions, respectively) and the change in the first-order natural frequency in the initial and end edge intervals, the building seemed to be heavily damaged by the main shock. The horizontal stiffness sharply dropped, and the damage in the *LG* direction was slightly larger than the damage in the *TR* direction.

3) According to the analysis of the ambient vibration records, the main cause of the large decrease in the first-order natural frequency prior to 2006 was probably the Miyagi-ken Nanbu Earthquake in 1998.

4) From the response records for the main shock and the change in frequency calculated from the ambient vibration records, the damage from the main shock for the *LG* direction was probably slightly more severe than that for the *TR* direction.

5) The damaged stories were estimated by using the mode shape curvature calculated from the eigenmodes before and after damage, and the results suggested that all the floors were similarly damaged. Based on the results in this study and past experimental studies, it is believed that the mode shapes have such a property that they vary slightly and globally if the building has local damage. However, it is unknown whether such a property can also be found in the building that was very severely damaged.

6) The damping system of the building can be evaluated as a proportional damping system as far as the lower modes are concerned. However, the applicability of the proportional damping system to a building that was more severely damaged is under investigation.

ACKNOWLEDGMENTS

The authors are grateful to NEWJEC Inc. (Technology Developing Group), NTT Facilities (Research & Development Headquarters), Yamanaka Laboratory of the Tokyo Institute of Technology, Nagano Laboratory of the Tokyo University of Science, and Toshinawa Laboratory of Meisei University for lending us portable accelerometers.

REFERENCES

1) Nakamura, Y. et al.: Research on Base Isolation System for Structure (Part 1: Outline of Research), Summaries of Technical Papers of Annual Meeting Architectural Institute of Japan. B, Structures I, 1987, pp. 767-768 (in Japanese).
2) Saruta, M. et al.: Research on Base Isolation System for Structure (Part 2: Indoor Experiments and Preparatory Tests), Summaries of Technical Papers of Annual Meeting Architectural Institute of Japan. B, Structures I, 1987, pp. 769-770 (in Japanese).
3) Okada, K. et al.: Research on Base Isolation System for Structure (Part 3: Earthquake Observation of Structures at Tohoku University), Summaries of Technical Papers of Annual Meeting Architectural Institute of Japan. B, Structures I, 1987, pp. 771-772 (in Japanese).
4) Tamura, K. et al.: Research on Base Isolation System for Structure (Part 4: Response Characteristics of Base Isolated Structure), Summaries of Technical Papers of Annual Meeting Architectural Institute of Japan. B, Structures I, 1987, pp. 773-774 (in Japanese).

5) Brincker, R., Zhang, L., and Andersen, P.: Modal Identification from Ambient Responses Using Frequency Domain Decomposition, *Proceedings of 18th International Modal Analysis Conference*, San Antonio, Texas, 2000, pp. 625-630.
6) Zhang, L.-M., Wang, T., and Tamura Y.: A Frequency-Spatial Decomposition (FSDD) Technique Operational Modal Analysis, *Mechanical Systems and signal Processing*, Volume 24, Issue 5, 2009, pp. 1227-1239 (in Japanese).
7) Iiyama, K. and Kurita, S.: Development of the Theory of Modal Identification for Proportional Viscous Damping System by Frequency Domain Decomposition, *Proceedings of AIJ Kinki Chapter Architectural Research Meeting*, 52, 2012, pp. 109-112 (in Japanese).
8) Recommendations for Aseismic Design and Construction of Nonstructural Elements (Second edition), Architectural Institute of Japan, 2008 (in Japanese).
9) *Shinsai Kenchikubutsu No Hisaido Kubun Hantei Kijun Oyobi Fukkyu Gijutsu Shishin* [*Standards for Postearthquake Damage Evaluation and Technical Guideline for Restoration for Damaged Buildings*], Second edition, The Japan Building Disaster Prevention Association, 2002 (in Japanese).
10) Katsukura, H. et al.: A Study on Drift Component of Displacement Obtained from Strong Motion Accelerograms Considering Causality of Seismic Waves, *Journal of Structural and Construction Engineering*, Volume 397, 1989, pp. 42-47 (in Japanese).
11) Hayashi, Y. et al.: Reliability of Integrated Displacements from Accelerograms by Digital Accelerographs, *Journal of Structural and Construction Engineering*, Volume 419, 1991, pp. 57-66 (in Japanese).
12) Cho K. : -Shingo Shori No Tame No Senkei Daisu- (Linear algebra for signal processing), Morikita Publishing Co., Ltd., 2008 (in Japanese)
13) Kondo, I. and Hamamoto, T.: Damage Detection of Multi-Storey Buildings Using Random Response Data from Shaking Table Tests, *Journal of Structural and Construction Engineering*, Volume 473, 1995, pp. 67-74 (in Japanese).
14) Saruta, M.: *Menshin Kouzoubutsu No Jishin Ji Anzensei Ni Kansuru Kenkyu* [*A Study on Safety of Isolated Building During Earthquake*], PhD Thesis, Tohoku University, Miyagi, Japan, 1999 (in Japanese).
15) Sato, T. et al.: Vibration Characteristics of Base Isolated Low Rise Building Based on Microtremor Measurements: Part 1 Comparison with Finite Element Method, Summaries of Technical Papers of Annual Meeting Architectural Institute of Japan. B-2, Structures II, Structural dynamics nuclear power plants, 2007, pp. 981-982 (in Japanese).
16) SEIN performance design series, Reference manual, Volume Calculation method, NTT Data (in Japanese).

(Original Japanese Paper Published: November, 2012)
(English Version Submitted: December 2, 2014)
(English Version Accepted: December 22, 2014)